Published in final edited form as:
J Neurosci. 2012 December 12; 32(50): 17948–17960. doi:10.1523/JNEUROSCI.1860-12.2012.

Cognitive deficits and delayed neuronal loss in a mouse model of multiple microinfarcts

Minghuan Wang[*,1,2], **Jeffrey J. Iliff**[*,1], **Yonghong Liao**[1], **Michael J. Chen**[1], **Matthew S. Shinseki**[1], **Arun Venkataraman**[1], **Jessica Cheung**[1], **Wei Wang**[2], and **Maiken Nedergaard**[1]

[1]Division of Glial Disease and Therapeutics, Center for Translational Neuromedicine, Department of Neurosurgery, University of Rochester Medical Center, Rochester, New York 14642

[2]Department of Neurology, Tongji Hospital, Tongji Medical College, Huazhong University of Science and Technology, Wuhan, China 430030

Abstract

Microinfarcts are a common clinical feature of the aging brain, particularly in patients with cognitive decline, vascular or Alzheimer's dementia. However, the natural history of these lesions remains largely unexplored. Here we describe a mouse (C57BL/6J) model of multiple diffuse microinfarcts induced by unilateral internal carotid artery injection of cholesterol crystals (40-70μm). Microinfarcts were spread throughout the deep cortex, subcortical tissue and hippocampus and were comprised of a CD68 (a marker for reactive microglia and macrophages)-positive core surrounded by large regions of GFAP-positive reactive astrogliosis. Widespread reactive gliosis, including mislocalization of the astrocytic water channel aquaporin-4 (AQP4) persisted long after injury, recovering only after 1 month post-stroke. Within the cortex, neuronal cell death progressed gradually over the first month, from ~35% at 3 days to 60% at 28 days post-stroke. Delayed demyelination was also observed in lesions, beginning 28 days post-stroke. These findings demonstrate that microinfarct development follows a distinct course compared to larger regional infarcts such as those induced by middle cerebral artery occlusion. The long-lasting gliosis, delayed neuronal loss and demyelination suggest that the therapeutic window for microinfarcts may be much wider (perhaps days to weeks) than for larger strokes.

Introduction

Numerous neuropathological and neuroimaging studies demonstrate that microinfarcts are surprisingly common in the aging brain (Brundel et al 2012). Within the broader aging population, incidence exceeds 30% (Brayne et al 2009, Vinters et al 2000, Xuereb et al 2000) while in elderly patients suffering from mild cognitive decline or dementia the rates are nearly twice as high. Patients with mild cognitive decline exhibit a microinfarct incidence of ~55% (Sonnen et al 2007) and a rate of 60-70% is reported among those suffering from vascular dementia (Erkinjuntti et al 1988, Esiri et al 1997, Haglund et al 2006). Demonstrating a causal relationship between cerebral microinfarcts and cognitive impairment, however, remains challenging because the literature is composed almost exclusively of community- or hospital-based autopsy studies focusing on elderly patients

Corresponding Authors: Jeffrey J. Iliff, PhD or Maiken Nedergaard, MD, PhD, Center for Translational Neuromedicine Box 645 601 Elmwood Avenue Rochester, NY 14642, USA. jeffrey_iliff@urmc.rochester.edu; nedergaard@urmc.rochester.edu Phone: (585) 273-2868 .
*These authors contributed equally to this study.

Disclosures: None.

(Brundel et al 2012), making it difficult to control for commonly-occurring risk factors such as diabetes and hypertension.

Experimental analysis of the pathophysiological events leading to neuronal loss in microinfarcts lags far behind work focused on larger focal or global cerebral ischemia. In the classic focal cerebral ischemia model, the middle cerebral artery occlusion (MCAO), the ischemic infarct extends uniformly through a large portion of the ipsilateral cortex and striatum. Within 3 hours of the onset of permanent ischemia, most of the potentially salvageable ischemic penumbra is absorbed into the infarct core and tissue injury is largely irreversible (Hossmann 2012). Within the core of the lesion, neuronal loss is complete within the first 24 hours after MCAO (Garcia et al 1995) while nearby astrocytes become reactive and form a rim surrounding the infarct core (Li et al 1995). Based upon the evolution of ischemic injury after permanent MCAO, the likely therapeutic window for salvaging at-risk neurons and tissue is exceedingly short (Hossmann 2012). In contrast, the microinfarcts associated with mild cognitive decline and vascular dementia are described most commonly as ‘microscopic’ (Brundel et al 2012), infiltrated with GFAP-positive reactive astrocytes and CD68-positive reactive microglia and macrophages (Erkinjuntti et al 1988, Haglund et al 2006, Okamoto et al 2009, Sonnen et al 2007). The evolution of these ischemic lesions remains largely undefined. Most importantly, it is not established whether neuronal death is limited to the first few hours of artery occlusion or whether it continues over a longer period. A more prolonged duration of neuronal loss in microinfarcts would not only suggest that the pathophysiological events are distinct, but also expand the therapeutic window for medical interventions. To begin to address these critical questions, well-defined and robust experimental models of diffuse microinfarction must be developed. Such models would also allow a better definition of the linkage between microinfarct development and cognitive decline.

We have here adapted a rat model of diffuse microinfarction (Rapp et al 2008) to mice and characterized the evolution of the ischemic lesions through the acute and chronic injury stages. In this model, we report the occurrence of two distinct lesion types, delayed neuronal loss and myelin disruption, in addition to long-term reactive astrocytosis and microgliosis, associated with cognitive impairment.

Methods

For all experiments, 8-10 week old (22-24g) male C57BL/6j mice (Charles River) and CX3CR1-GFP transgenic mice (Strain B6.129P-*Cx3cr1*^{tm1Litt}/J, JAX; backcrossed to Charles River C57BL/6j mice for 5 generations) were used. All experiments were approved by the institutional Animal Care and Use Committee of the University of Rochester and carried out according to guidelines from the National Institutes of Health.

Diffuse ischemia model

Cholesterol crystals (Sigma) sized 40-70μm were collected as described by Rapp et al. (Rapp et al 2008) with the minor modifications described below. Free cholesterol crystals were filtered through 70μm then 40μm cell strainers, then collected and counted with a hemocytometer.

Mice were randomly allocated into stroke and sham groups and anesthetized with ketamine and xylazine (50mg/kg and 10mg/kg ip) (Simard et al 2006, Wu et al 2012). The right common carotid artery (CCA), internal carotid artery (ICA) and external carotid artery (ECA) were carefully isolated under a dissecting microscope. The extracranial branch of the ICA was ligated with a 7-0 suture and the distal portion of the ECA was permanently ligated. Microvascular clips were applied to the CCA, the proximal part of the ECA and ICA

and an incision was made between the ECA ligation site and the ECA clip. Polyethylene (PE10) tubing was inserted into the ECA towards the CCA and the microvascular clips were removed to restore blood flow. 3000±500 cholesterol crystals in 100μl saline or 100μl saline alone (for sham animals) were injected via the PE10 tubing. After injection, the tube was removed and the proximal ECA was permanently ligated and the wound closed. Following stroke induction, animals were alert and moving within 2 hours and were closely monitored for the first 12 hrs following stroke.

Quantitative Immunohistochemistry

3, 14 or 28 days after surgery, stroke- or sham-treated animals were perfusion-fixed with 4% paraformaldehyde. After overnight post-fixation, 100μm vibratome brain slices were cut, washed, and blocked with 3% normal donkey serum in PBS with 0.01% Triton-X. Slices were incubated with one, two or three of the following primary antibodies: mouse anti-glial fibrillary acidic protein (GFAP, 1:1000; Millipore), rabbit anti-GFAP (1:1000, Sigma), rat anti-CD68 (1:100, Serotec), rabbit anti-aquaporin 4 (AQP4, 1:500; Millipore), mouse anti-NeuN (1:200, Millipore), mouse anti-myelin basic protein (MBP, 1:1000; Covance), rabbit anti-platelet endothelial cell adhesion molecule (PECAM-1 (CD31), 1:200; Abcam),rabbit anti Caspase-3 (1:500;Abcam). Secondary detection was carried out with Cy2-, Cy3- or Cy5-conjugated donkey anti-rabbit, mouse, or rat antibodies (1:500, Jackson Immunoresearch). Slices were mounted with Prolong Antifade Gold with DAPI (Invitrogen) and imaged by laser scanning confocal microscopy (FV500, Olympus). All images were acquired under the same imaging parameters (laser power, photomultiplier tube voltage and gain).

Consecutive 1mm and 100μm slices from stroke-treated brains were subjected to 2, 3, 5-triphenyltetrazolium chloride (TTC) labeling and immunolabeling, respectively, 24hrs after injury. 1mm slices were incubated in 2% TTC (Sigma) at 37°C for 15 minutes, then photographed. 100μm slices were immunolabeled against GFAP and CD68 as above and imaged by laser scanning confocal microscopy. 3, 14, 28 days post-injury, the diffuse stroke mice were perfusion-fixed with 4% paraformaldehyde. After overnight post-fixation and cryopreservation, 20μm cryostat sections were cut and hematoxylin/eosin (H&E) staining was conducted.

To determine what proportion of the cortical and striatal microvasculature was occluded in the present diffuse microinfarction model, 1 hr after induction of diffuse ischemia, FITC-conjugated lectin (Sigma) was injected into the blood stream via a femoral artery catheter at a dosage of 7.8 μmol/g (Chang et al., 2000). 30 minutes post-injection, the animal was perfusion-fixed, 100μm vibratome brain slices were cut and counter-labeled with anti-CD31 antibody. Five 40X confocal images were acquired randomly from both the contralateral and ipsilateral cortex and striatum (20 images per slice). Four slices were imaged in this way from each of 4 diffuse microinfarct- or sham-treated animals. Image analysis was conducted with ImageJ software. The total CD31-positive area of each image was calculated and a CD31-positive mask was generated. The lectin-positive area of the CD31-positive mask was calculated, and expressed as a % of CD31-positive area. Double-positive regions corresponded to perfused vessels, while CD31-positive/lectin-negative areas corresponded to occluded vessels. The person performing image acquisition and image analysis was blinded to the experimental group of the slice.

Characterization of microinfarcts

3, 14 and 28 days after stroke induction, brains were fixed and sliced. 100μm slices were serially distributed into four groups for immunolabeling: 1) GFAP and CD68 alone, 2) GFAP, CD68 and NeuN, 3) GFAP, CD68 and MBP, 4) GFAP, CD68 and AQP4. Slices

were mounted and imaged by epifluorescence (for whole-slice montage generation) or laser scanning confocal microscopy. For whole slice montage generations, slices were imaged at 4X objective power and montages were generated using Microlucida software (Microbrightfield). All slice montages were acquired under the same imaging parameters (exposure and gain). Confocal images were generated at 40X objective power and imaging parameters (photomultiplier tube voltage, gain) were maintained constant across compared groups. All image analysis was conducted with ImageJ software (NIH) and the person conducting image analysis was blinded to treatment group.

In slices labeled for GFAP and CD68 alone, CD68- and GFAP-immunoreactivity was first measured. The slice montage images were uniformly thresholded and the % coverage of the ipsilateral hemisphere, cortex (Ctx), subcortical regions (striatum and thalamus, SCtx), hippocampus (Hipp), and subcortical white matter (WM) were calculated for CD68 and GFAP in each region. Values for each slice within an individual animal were integrated, the result being reported a single biological replicate. CD68 or GFAP labeling was compared between regions or at different time points by one-way analysis of variance (ANOVA) with Tukey's post-hoc test to evaluate differences between individual groups.

Discrete CD68-positive lesions were counted and their relative distribution between different brain regions determined. A total of 116, 121 and 109 lesions were catalogued from animals 3 (n=7 animals), 14 (n=7 animals) and 28 (n=8 animals) days post-stroke, respectively. The CD68-positive lesion cores were projected to one of three representative anatomical brain slices to generate a lesion distribution map. Based on early analysis, we observed that lesions fell into two broad morphological classes: diffuse 'incomplete' lesions and dense 'cavitated' lesions. We tabulated the frequency of these lesion types within each brain region. The area of each lesion was calculated and plotted as a function of brain region, or time after stroke. The effect of brain region on lesion size was analyzed by one-way ANOVA, with Tukey's post-hoc test for comparison of individual groups. Differences in lesion size by lesion type and by time post-stroke were analyzed by a 2-way ANOVA with Bonferroni's post-hoc test to compare differences between individual groups.

In slices labeled for GFAP, CD68 and the neuronal cell body marker NeuN, neuronal loss after stroke was quantified in both the cortex and striatum. Confocal images were generated at 40X objective power (211×211μm) in regions centering on CD68- and GFAP-positive lesions and in mirror-image regions in the un-affected contralateral hemisphere. All NeuN-positive neurons within the imaging frames were counted in a blinded manner; image acquisition and counting were performed by different individuals. Counts were represented as the ipsilateral (lesion):contralateral (un-affected) ratio. Images were also generated 200μm from the lesion center, in regions that are CD68-negative but GFAP-positive. NeuN-positive neurons were counted. Neuronal counting was also conducted based upon lesion type. All lesions were divided into two groups, incomplete lesions and cavitated lesions, based upon the density of CD68 labeling and the presence of a defined GFAP-positive glial scar. NeuN-positive neurons were counted in these two different types of lesions using the method described above. Differences in ipsilateral:contralateral neuronal count ratios 3, 14 and 28 days after stroke were compared to control values by 1-way ANOVA with Dunnett's post-hoc test for multiple comparisons.

In slices labeled for GFAP, CD68 and the myelin marker MBP, myelin disruption after diffuse stroke was measured. Confocal images centering on CD68- and GFAP-positive lesions were generated as above. The color channels were separated and the MBP channel was uniformly thresholded and converted to a binary image. The length of discrete continuous MBP-positive pixel regions was calculated and averaged in an automated fashion (ImageJ) to derive a mean arbitrary value for 'myelin continuity' for each image (Figure

8E). These values were expressed as the ipsilateral:contralateral myelin continuity ratio and compared between control, 3, 14 and 28 days post-stroke as above.

In slices labeled for GFAP, CD68 and the astrocytic water channel AQP4, mean AQP4 immunoreactivity was first calculated. Confocal images centering on CD68- and GFAP-positive lesions were generated as above. The color channels were separated and the mean fluorescence intensity was calculated for each image. We also calculated the AQP4 expression polarity for each image. In this case, the color channels were separated and each image was thresholded uniformly at 2 different levels – a high and a low stringency threshold. The low-stringency threshold defined the overall area of AQP4-immunoreactivity while the high-stringency threshold defined the area of intense AQP4-immoreactivty that in control mice is localized to perivascular endfeet. The ratio of the low stringency area:high stringency area was used to generate an arbitrary value defining 'AQP4 polarity' (Figure 9E). The higher the AQP4 polarity, the greater proportion on immunoreactivity was restricted to perivascular regions, while the lower the proportion the more evenly distributed immunoreactivity was between the perivascular endfeet and the soma. AQP4 polarity values were expressed as the ipsilateral:contralateral ratio and compared between control, 3, 14 and 28 days post-stroke as above. Differences at 3, 14 and 28 days were compared to control values by 1-way ANOVA with Dunnett's post-hoc test for multiple comparisons.

Brain water content measurement

3 days post-stroke, anesthetized sham and stroke mice were decapitated and brains were dissected and immediately weighed. Brains were kept at 65°C for 48 hours until they reached a constant weight. Brains were re-weighed and the brain water content was measured as follows:

$$\%\text{water content} = 100\% \times (\text{wet weight} - \text{dry weight}) / \text{wet weight}$$

Differences in brain water content between sham and stroke groups were compared by unpaired *t*-test (n=6 per group).

Intracranial pressure measurement

3 days after stroke, a small burr hole was drilled with a dental drill in the center of the parietal bone and the dura was punctured carefully to avoid damage to the underlying brain tissue. The pressure sensor (Millar Instruments) was inserted 300μm into the cortex and the burr hole and probe were sealed and secured with dental cement. The ICP signal was digitized and recorded with a DigiData 1332A and PClampex9.2 software (Axon Instruments). The mouse was allowed to stabilize for 15min, then intracranial pressure (ICP) was recorded continuously for 5min. The mean value was recorded as the animal's ICP. Comparison between sham and stroke values was made by unpaired *t*-test (n=6 per group).

Blood brain barrier function

3 days after surgery, sham- and stroke-treated animals were anesthetized and 15μl 1% ALEXA647-conjugated ovalbumin (OA647, MW 45kD) was injected into the blood through a femoral arterial catheter. 30min after injection, animals were perfusion-fixed, brains sliced, and slices immunolabeled as above for GFAP and CD68. Lesions were identified by CD68- and GFAP-immunoreactivity, and OA647 extravasation was imaged in and around defined lesions and was compared to mirror image un-affected contralateral tissue (n=3 sham, 3 stroke).

Evaluation of cognitive function following diffuse ischemic injury

For all behavioral tests, the person conducting the test and the person coding behavioral data were blinded to treatment group. To evaluate whether induction of ischemic injury resulted in cognitive impairment, animals were subjected to the novel object recognition and contextual fear conditioning tests. The novel object recognition test was performed weekly after stroke or sham surgery according to the method described previously, with certain modifications (Antunes & Biala 2011, Ennaceur 2010, Ennaceur & Delacour 1988). The experiments were carried out over 2 consecutive days in a plastic cage (50cm x 25cm x50cm) with camera attached. Mice were habituated to the test box for 10 min one day before the exploration session. In the first day, two identical objects were introduced in two corners (approximately 30 cm apart from each other) and the time spent exploring each object was recorded during a 5 min period (defined as the training session). In the second day, the mice were placed in same test environment while one of the familiar objects used in the previous training session was replaced with a novel object. The time spent exploring each object was recorded during a 5 minutes period, which defined as the test session. The animals were regarded to be exploring when they were facing, sniffing or biting the object. The test box and objects were cleaned with 70% of ethanol between trials. A ratio of the time that mice spent exploring each objects in a whole 5 minutes period during the training session and a ratio of the time that the mice spent exploring each object in the first minute during the test were used to measure memory preference.

The contextual fear conditioning test was performed according to the method described previously with certain modifications (Gould 2003, Gould & Lommock 2003). 14 and 28 days after surgery, mice were introduced into the test chambers and baseline freezing behavior was assessed for 120s. An auditory conditioning stimulus was introduced with a 2s 0.3mA shock stimulus (delivered through metal rods in the floor), which was repeated once after 120 seconds. This defined the training session. On the second day, the freezing behavior was re-assessed under the same paradigm, excepting that no shock was administered through the chamber floor. Animals exhibiting greater freezing behavior in response to the conditioned stimulus were regarded to have exhibited greater learning behavior. The evolution of cognitive deficits over time was compared between sham- and stroke-treated animals by 2-way ANOVA with Bonferroni's post-hoc test for multiple comparisons.

Mice were also subjected to an open field test to evaluate the presence of general motor deficits. Mice were tested 7 and 14 days following induction of diffuse stroke or sham operation. The test procedure was as described previously (Silverman et al 2007) with modifications. Mice were placed in the open field apparatus (40×40×30 cm, opaque plastic walls) with an attached camera that recorded mouse activity. Mice were placed in the area to become familiar with the environment for 1min, then were allowed to explore freely for 10min. The distance traveled in the arena and time spent in the central and peripheral regions were recorded over the test session. Mouse activity during 10min test period was analyzed using Any-Maze software (Stoelting).

Statistical Analysis

Data are presented as mean ± SEM. All statistics were performed using Prism software (Graphpad). The specific statistical tests used to compare different types of data are detailed with the methodological description. A P value <0.05 was considered statistically significant.

Results

Initial characterization of diffuse embolic stoke model and lesions

We first characterized the resulting lesion burden 3 days after induction of diffuse ischemic injury. After unilateral injection of cholesterol crystals into the internal carotid artery (Figure 1A), small, well-defined lesions were apparent scattered largely unilaterally (<90% ipsilateral to the injection site) throughout the cortex, striatum, hippocampus and subcortical white matter. These lesions were readily detectable by immunolabeling for CD68 (a marker for reactive microglia and macrophages) and were surrounded by extended regions of GFAP-positive reactive astrogliosis (Figure 1B). H&E staining conducted 3 days post-injury demonstrated abundant macrophage infiltration into the lesion sites (Figure 1C-D, Figure 2A-C). Immunolabeling of consecutive slices for GFAP and CD68 revealed that lesions detectable by H&E staining corresponded to CD68-positive lesions that were surrounded by reactive astrogliosis (Figure 1E). We observed that CD68-positive labeling co-localized with Iba1 expression (Figure 3A), and with endogenous GFP expression in CX3CR1-GFP reporter mice (Figure 3B). Thus, the CD68-positive core of the observed microinfarcts corresponds with the presence of reactive microglia and macrophages.

When immunolabeling and TTC staining were conducted in consecutive brain slices 24 hours after diffuse ischemic injury, lesions identified by TTC labeling (Figure 1F) were surrounded by a rim of reactive microglia and astrocytes (Figure 1G-H). The TTC lesions differed from those conventionally observed for more regional ischemic insults in that they were smaller and did not appear completely white. This is likely the result of the incomplete nature of these diffuse lesions. At this early time point, CD68 labeling was not observed within the interior of the infarct, which is consistent with the occurrence of macrophage invasion into the infarct beginning >24hrs after ischemic injury (Gelderblom et al 2009).

Overall lesion (defined as CD68-positive regions) burden of the ipsilateral hemisphere was ~11% of the total hemispheric volume (Figure 1I**,** n=8 animals). The largest numbers of lesions were present in the cortex and striatum, with fewer observed in the hippocampus and only a small number of lesions apparent in the subcortical white matter tracks of the corpus callosum, internal and external capsules (Figure 5A-B). Lesion coverage and size did not differ between the cortex and subcortical regions, while hippocampal lesions were both larger (Figure 5C; *P < 0.05 vs. Ctx and SCtx, ANOVA) and occupied a greater proportion of tissue volume (Figure 1I; *P < 0.05 vs. other regions, ANOVA). This may suggest that within the hippocampus, smaller individual lesions have merged to form larger compound lesions.

When we evaluated the extent of microvascular occlusion that resulted from diffuse microinfaction, we found that in the hemisphere ipsilateral to the cholesterol injection, ~30% of the microvasculature was not perfused (was not labeled by iv lectin, Figure 4A-B; *P<0.05 vs. Control values, ANOVA). The regions of non-perfusion were typically small and spread widely throughout the cortex and striatum. Consistent with the observation that lesion burden did not significantly differ between these two regions (Figure 1I), the proportion of perfused microvasculature did not differ between ipsilateral cortex and striatum (Figure 4B). We observed no appreciable microvascular occlusion in the hemisphere contralateral to cholesterol injection. This is consistent with the fact that >90% of observed lesions appeared in the ipsilateral hemisphere.

At 3 days following diffuse stroke, two morphologically distinct lesion types were observed: diffuse ‘incomplete’ lesions and dense ‘cavitated’ lesions (Figure 5E-F). Incomplete lesions were irregularly-shaped areas of CD68-positive reactive microgliosis intermingled with and surrounded by GFAP-positive reactive astrocytes (Figure 5E). Cavitated lesions were ~2.5X

larger than gliotic lesions (Figure 5D) and had a well-defined lesional core that was filled with CD68-positive invading cells and was devoid of astrocytes (Figure 5F). Cavitated lesions were immediately bounded by a rim of reactive astrocytes, and as with incomplete lesions, were surrounded by extended regions of reactive gliosis. Cavitated lesions were more commonly observed in the hippocampus or within deeper portions of the sub-cortex, while they were not observed within the white matter (Figure 5G).

Three days after diffuse stroke injury, mild cerebral edema was apparent within affected animals. Whole brain water content was significantly increased from 76.9 ± 0.4% in sham-treated mice to 78.6 ± 0.4% in stroke-injured animals (Figure 6A, *P<0.05 *t*-test, n=6 each group). ICP measured within the ipsilateral cortex was also slightly elevated from 22.1 ± 1.3 mmH_2O in sham animals to 26.3 ± 1.3 mmH_2O in animals following diffuse stroke injury (Figure 6B**,** *P < 0.05 *t*-test, n=6 each group). Highly-localized blood brain barrier disruption was observed 3 days after injury (Figure 6C-E, n=3 replicates). Following intravenous infusion of Alexa647-conjugated ovalbumin (OA-647, MW 45kD), tracer extravasation into the parenchyma of mice following diffuse ischemia was evident in areas of CD68-immunoreactivity. The extent of blood brain barrier disruption corresponded to lesion size, with small gliotic lesions exhibiting only limited disruption (Figure 6C-D) while large lesions exhibited pronounced blood brain barrier dysfunction (Figure 6E). Similar results were observed when FITC-conjugated dextran (MW 3kD) was used to probe blood brain barrier disruption (not shown, n=3 replicates).

We next evaluated the evolution of these ischemic lesions in the chronic stage, including 14 and 28 days after the induction of diffuse ischemic injury. When evaluated by H&E staining, 2 weeks post-stroke widespread fibrillary gliosis was evident within and surrounding incomplete lesions while pyknotic neurons were plainly evident (Figure 2D-F). At the same time point, the CD68-positive lesion burden was significantly reduced, from ~10% to ~3% of the ipsilateral hemisphere (Figure 1J; *P <0.05 ANOVA, n=7 animals). The average size of incomplete lesions was reduced by more than 50% (Figure 5D; *P<0.05 vs. value at 3 days, ANOVA, n=7 animals) while the sizes of cavitated lesions were not significantly altered. Thus, the stabilization of CD68-positive lesions at 14 days was driven largely by consolidation of incomplete, rather than cavitated lesions. 28 days post-injury, many lesions were characterized by glial scarring and internal cavitation (Figure 2G-I). Compared to the dynamics of microgliosis after diffuse stroke injury, the resolution of reactive astrogliosis was more protracted, with significant reductions GFAP labeling only occurring after 28 days (Figure 1J; *P<0.05 vs. value at 3 days, ANOVA).

Evaluation of neuronal loss following diffuse stroke

We next tested whether the incomplete lesions and long-lasting gliosis caused by diffuse ischemic injury resulted in delayed neuronal death. CD68- and GFAP-positive lesions were identified 3, 14 and 28 days after ischemic injury. Neurons within the CD68- and GFAP-positive core were counted based on NeuN (neuronal nuclear antigen) labeling and normalized to counts obtained from mirror-image regions of the un-affected contralateral hemisphere. Within the cortex, lesions exhibited time-dependent neuronal death, from ~35% at 3 days, to ~55% at 14 days to ~60% at 28 days (Figure 7B, E-F, H-I; *P<0.05 vs. Control, ANOVA, n = 5-6 animals). Importantly, statistically-significant differences in neuronal counts were observed between 3 days and 14 or 28 days (**P<0.05). Within subcortical regions, significant neuronal death was also observed following diffuse ischemic injury (Figure 7B; *P<0.05 vs. Control, ANOVA), however neuronal loss at 3 days (~50%) was not significantly different than at 14 or 28 (~65%) days post-stroke. When neurons were counted 200μm from the lesion center, a region that exhibited GFAP-but not CD68-

immunoreactivity, low-level (~5-8%) neuronal loss was observed in the cortex beginning at 3 days post-injury (Figure 7D; *P<0.05 vs. Control, ANOVA).

Analysis of neuronal loss based upon the type of lesion (incomplete vs. cavitated) revealed a striking difference between incomplete and cavitated lesions. Cavitated lesions exhibited a more rapid and complete neuronal loss than did incomplete lesions, which underwent neuronal loss more gradually (Figure 7C). In cavitated lesions, neuronal loss appeared to be complete within 14 days post-injury. In contrast, even at 28 days post-injury, neuronal loss within incomplete lesions was still ongoing. When caspase-3/NeuN double-labeling was conducted, neuronal caspase-3 labeling remained evident within incomplete lesions 14 and 28 days post-injury (Figure 7G, J), confirming that apoptotic neuronal loss was still occurring at these late time points. Thus, following diffuse microinfarction, two distinct lesion types appear to evolve over markedly different trajectories: cavitated lesions exhibit stable lesion boundaries, complete glial scars, and rapid neuronal loss; incomplete lesions exhibit a slowly-resolving reactive gliosis and ongoing neuronal loss.

Characterization of glial dysfunction following diffuse ischemic injury

In light of this persistent reactive gliosis and delayed neuronal loss, we surmised that myelination might be disrupted following diffuse ischemic insult. MBP labeling was conducted in brain slices 3, 14 and 24 days after induction of ischemic injury (Figure 8A-D). Within CD68- and GFAP-positive lesions and un-affected contralateral tissue, myelin organization was analyzed and a value reflecting MBP continuity was derived as described (Figure 8E). Compared to control slices, myelin continuity was significantly reduced only at 28 days post-stroke (Figure 8F; *P<0.05 vs. Control, ANOVA, n=5-6 animals). Changes in myelination were observed in individual lesions at 3 and 14 days after injury, but these were inconsistent across the broader population of lesions (reflected in the higher variance in continuity values).

Following diffuse ischemic injury, widespread reactive astrogliosis was apparent 14 days after stroke (Figure 1J) and remained detectable around lesion foci 28 days after injury. (Figure 8D, 9D). One of the central functions of astrocytes following injury is the appropriate distribution of water within brain tissue, so we next evaluated the expression and polarization of AQP4 at 3, 14 and 24 days post-stroke (Figure 9A-D). Overall AQP4 expression levels in CD69- and GFAP-positive lesions were significantly increased 3 days following injury (Figure 9F; *P<0.05 vs. Control, ANOVA, n=5-6), but returned to baseline levels by 14 days post-stroke. Under physiological conditions, AQP4 expression is highly polarized to perivascular astrocytic endfeet, where it is presumed to mediate fluid entry into and efflux from the CNS. In addition to quantifying overall expression, we measured AQP4 expression polarity as described (Figure 9E) and compared it to un-affected contralateral tissue. 3 and 14 days post-stroke, AQP4 polarity was significantly reduced (Figure 9G; *P<0.001 vs. Control, ANOVA). By 28 days post-stroke, AQP4 polarity was no longer significantly different from control values (Figure 9G). Thus, in addition to ongoing neuronal loss, the present diffuse ischemic injury model also results in both delayed failure of myelination and disruption on astrocytic AQP4 polarization in and around lesion foci.

Measurement of cognitive decline following diffuse ischemic insult

We last evaluated changes in cognitive function after induction of diffuse ischemic injury. Mice were tested in the Novel Object Recognition test weekly following stroke and compared to sham-operated controls. At 7 and 14 days following stroke, injured animals exhibited significantly reduced preference for the novel object (Figure 10A; *P<0.05 vs. Sham, ANOVA, n=10 sham, 15 stroke group), indicating compromise of cognitive function. Between 21 and 28 days post-stroke, function within the novel object recognition test

returned to normal values. A second cognitive test was utilized in animals either 14 or 28 days after diffuse ischemic injury. Evaluation of hippocampal- and amygdala-based learning by contextual and tonal fear conditioning, respectively, revealed significant hippocampal-dependent cognitive deficits in animals 14 days following stroke (Figure 10B; *P<0.05 vs. Sham, ANOVA, n=10 per group) while amygdala-based learning was not impaired. Hippocampus-dependent cognitive deficit was not apparent in animals 28 days following injury. Using the open field test, no significant difference in either path traveled (a measure of gross motor function) or the percentage of time spent in the middle portion of the test arena (a measure of anxiety) were observed between diffuse stroke- and sham-treated mice at either 7 or 14 days post-injury.

Discussion

Microinfarcts are common features among elderly patients, particularly those suffering mild cognitive decline or from vascular or Alzheimer's dementia (Brundel et al 2012) and are thought to play a causal role in age-related cognitive decline. However, the time course of individual and aggregate lesion development remains largely obscure because the microscopic infarcts are typically first identified only upon post-mortem examination. Although several models of microinfarction exist in rats (Bailey et al 2009, Rapp et al 2008), to our knowledge this is the first mouse model of diffuse microinfarction to be developed and more broadly, the first study to provide a detailed characterization of microinfarct lesion development through the acute and chronic phases. We describe that the lesions produced within this model match those observed in clinical populations in terms of size, distribution and histological characteristics. These lesions are complex in their evolution, exhibiting delayed neuronal cell death and demyelination in addition to spatially widespread and prolonged astrogliosis. Importantly, we identify two distinct histologically-distinct lesion types, cavitated and incomplete lesions, that evolve along markedly different trajectories.

In neuropathological studies from human patient populations, microinfarcts are characterized as lesions of varying shape, including 'slit-like, triangular, round, barrel-shaped, stellate, granular to wedge-shaped', <1-2mm in size and distribute widely throughout cortical and subcortical regions (for a detailed review of microinfarcts in human neuropatholigical studies, see (Brundel et al 2012)). While traditional focal ischemic lesions are defined as necrotic regions exhibiting a loss of all cell types, microinfarcts described in the human clinical literature are incomplete and diffuse, associated with invading CD68-positive macrophages and reactive microglia in addition to reactive astrocytes. One key finding of the present study was that the lesions generated in the mouse model closely resembled the neupopathological findings in human brains. Lesions were observed of varying shape, although roughly round (Figure 1B, F) and columnar or wedge-shaped lesions (Figure 1C, 6C) were observed most commonly. Lesion cores were associated with CD68-positive reactive microglia and macrophages, were typically microscopic (<1mm), distributed throughout the deep cortex and subcortical tissues, and were associated widespread reactive astrogliosis. Thus the present mouse diffuse stroke model recapitulates the hallmark characteristics of human microinfarcts.

The present observation that intra-arterial cholesterol crystal injection can be used to reliably generate diffuse microinfarction is in contrast to a prior study in which a similar methodology produced consistent cortical spreading depression, but only inconsistent microinfarction (Nozari et al 2010). Important methodological differences likely account for these discrepancies. First, Nozari et al. utilized a similar number of cholesterol crystals filtered to include those <70μm in diameter, while we utilized a double-filtration technique to include only those crystals *between* 40 and 70μm. This likely resulted in the occlusion of larger upstream microvessels (typically deep penetrating arterioles) in our model. A second

key difference lay in the histological methods used to identify microinfarcts. The prior study used H&E staining and magnetic resonance imaging to identify ischemic lesion formation 72 hours post-injury. We found that the lesion cores (defined as regions of CD68-positive reactive microgliosis and macrophage infiltration), constituted only a small fraction of the gliotic lesion that was evident upon immunolabeling with GFAP. For this reason, in our hands H&E labeling was markedly inferior to CD68/GFAP double-labeling for the detection of diffuse gliotic lesions. The occurrence of delayed neuronal loss in this model also may have prevented the detection of pyknotic neurons 72 hours post-injury in the prior study (Nozari et al 2010).

One key benefit for an animal model of diffuse ischemic injury is the ability to study the natural history of individual lesions from the time of induction into the chronic phase, which is not possible in neuropathological studies in humans. Immediately following the ischemic episode induced by intracarotid injection of cholesterol crystals, mild cerebral edema and highly localized blood brain barrier disruption was observed. The lesion could typically be separated into two histologically distinct regions, including a CD68-positive core and a large surrounding region of GFAP-positive reactive astrogliosis. Interestingly, these two regions appeared to evolve on differing timescales. The central CD68-poitive lesion consolidated between 7 and 14 days post-injury to achieve an apparently stable size. In contrast, resolution of reactive astrogliosis was more protracted and did not occur until 28 days post-stroke. This was true not only of GFAP-immunoreactivity (a classical marker for reactive gliosis), but also of AQP4 polarization within perivascular endfeet, suggesting that astroglial function, including water homeostasis and edema clearance (Saadoun & Papadopoulos 2010, Zador et al 2009), may be compromised for a long period of time within a wide region surrounding these diffuse ischemic lesions.

Through the ability to track lesion development from the acute to the chronic phase, we were able to identify two histologically-distinct classes of lesions: cavitated and incomplete lesions. Cavitated lesions appeared to be very small, conventional necrotic ischemic lesions. The lesion site was complete, bounded by a stable glial scar that did not significantly change in dimensions between 3 and 28 days post-injury. Neuronal loss within these lesions was rapid, and apparently complete within the first 14 days post-injury, after which these lesions became cystic cavities. These ‘conventional’ ischemic lesions, however, represented only a small fraction of the lesion burden in the present diffuse microinfarction model. In agreement with observed human microinfarcts (Brundel et al 2012), the dominant lesion type observed in the present model were incomplete lesions. These lesions exhibited widespread reactive astrogliosis, but no defined glial scar. Surrounding astrogliosis was less stable, consolidating gradually over the course of the 28 days post-injury. Importantly, neuronal loss within these gliotic lesions was delayed and appeared to be occurring on an ongoing basis.

The presence of delayed neuronal loss and demyelination following diffuse microinfarction is a critical finding. Within the classical MCAO ischemia model, ischemic cell death is largely irreversible within 3 hours (Hossmann 2012) and is complete within 24 hours after injury (Garcia et al 1995). In the observed incomplete lesions, neuronal loss was progressive between 3, 14 and 28 days post-stroke. Evan at 28 days post-injury, caspase-3-positive neurons could be identified within incomplete lesions. This suggests that the neurons are not being lost solely during the initial ischemic insult, but rather as a result of delayed processes that may differ fundamentally from those of acute ischemic events. Similar results were obtained when myelination was assessed by MBP labeling. Although sporadic changes in myelination were observed in a subpopulation of lesions at 3 and 14 days post stroke, significant and wide-spread demyelination was not apparent in incomplete ischemic lesions until 28 days post stroke. This demonstrates that critical differences exist between the

evolution of incomplete microinfarcts and larger regional infarcts represented by the MCAO and similar models. Insufficient metabolic support from reactive astrocytes, inflammatory processes, and BBB opening could all contribute to the delayed neuronal loss. Most importantly, this observation suggests that the therapeutic window to intervene clinically to protect cells associated with these diffuse ischemic lesions may be considerably wider than for larger infarcts, perhaps extending to days and weeks after the initial insult.

Acknowledgments

This work was supported by the National Institutes of Health, the United States Department of Defense, and the Harold and Leila Y. Mathers Charitable Foundation.

References

Antunes M, Biala G. The novel object recognition memory: neurobiology, test procedure, and its modifications. Cognitive processing. 2011

Bailey EL, McCulloch J, Sudlow C, Wardlaw JM. Potential animal models of lacunar stroke: a systematic review. Stroke; a journal of cerebral circulation. 2009; 40:e451–8.

Brayne C, Richardson K, Matthews FE, Fleming J, Hunter S, et al. Neuropathological correlates of dementia in over-80-year-old brain donors from the population-based Cambridge city over-75s cohort (CC75C) study. J Alzheimers Dis. 2009; 18:645–58. [PubMed: 19661624]

Brundel M, de Bresser J, van Dillen JJ, Kappelle LJ, Biessels GJ. Cerebral microinfarcts: a systematic review of neuropathological studies. J Cereb Blood Flow Metab. 2012; 32:425–36. [PubMed: 22234334]

Chang YS, di Tomaso E, McDonald DM, Jones R, Jain RK, Munn LL. Mosaic blood vessels in tumors: frequency of cancer cells in contact with flowing blood. Proceedings of the National Academy of Sciences of the United States of America. 2000; 97:14608–14613. [PubMed: 11121063]

Ennaceur A. One-trial object recognition in rats and mice: methodological and theoretical issues. Behavioural brain research. 2010; 215:244–54. [PubMed: 20060020]

Ennaceur A, Delacour J. A new one-trial test for neurobiological studies of memory in rats. 1: Behavioral data. Behavioural brain research. 1988; 31:47–59. [PubMed: 3228475]

Erkinjuntti T, Haltia M, Palo J, Sulkava R, Paetau A. Accuracy of the clinical diagnosis of vascular dementia: a prospective clinical and post-mortem neuropathological study. Journal of neurology, neurosurgery, and psychiatry. 1988; 51:1037–44.

Esiri MM, Wilcock GK, Morris JH. Neuropathological assessment of the lesions of significance in vascular dementia. Journal of neurology, neurosurgery, and psychiatry. 1997; 63:749–53.

Garcia JH, Liu KF, Ho KL. Neuronal necrosis after middle cerebral artery occlusion in Wistar rats progresses at different time intervals in the caudoputamen and the cortex. Stroke; a journal of cerebral circulation. 1995; 26:636–42. discussion 43.

Gelderblom M, Leypoldt F, Steinbach K, Behrens D, Choe CU, et al. Temporal and spatial dynamics of cerebral immune cell accumulation in stroke. Stroke; a journal of cerebral circulation. 2009; 40:1849–57.

Gould TJ. Ethanol disrupts fear conditioning in C57BL/6 mice. J Psychopharmacol. 2003; 17:77–81. [PubMed: 12680742]

Gould TJ, Lommock JA. Nicotine enhances contextual fear conditioning and ameliorates ethanol-induced deficits in contextual fear conditioning. Behavioral neuroscience. 2003; 117:1276–82. [PubMed: 14674846]

Haglund M, Passant U, Sjobeck M, Ghebremedhin E, Englund E. Cerebral amyloid angiopathy and cortical microinfarcts as putative substrates of vascular dementia. International journal of geriatric psychiatry. 2006; 21:681–7. [PubMed: 16802283]

Hossmann KA. The two pathophysiologies of focal brain ischemia: implications for translational stroke research. J Cereb Blood Flow Metab. 2012

Li Y, Chopp M, Zhang ZG, Zhang RL. Expression of glial fibrillary acidic protein in areas of focal cerebral ischemia accompanies neuronal expression of 72-kDa heat shock protein. Journal of the neurological sciences. 1995; 128:134–42. [PubMed: 7738589]

Nozari A, Dilekoz E, Sukhotinsky I, Stein T, Eikermann-Haerter K, et al. Microemboli may link spreading depression, migraine aura, and patent foramen ovale. Annals of neurology. 2010; 67:221–9. [PubMed: 20225282]

Okamoto Y, Ihara M, Fujita Y, Ito H, Takahashi R, Tomimoto H. Cortical microinfarcts in Alzheimer's disease and subcortical vascular dementia. Neuroreport. 2009; 20:990–6. [PubMed: 19483658]

Rapp JH, Hollenbeck K, Pan XM. An experimental model of lacunar infarction: embolization of microthrombi. J Vasc Surg. 2008; 48:196–200. [PubMed: 18486421]

Saadoun S, Papadopoulos MC. Aquaporin-4 in brain and spinal cord oedema. Neuroscience. 2010; 168:1036–46. [PubMed: 19682555]

Silverman MN, Macdougall MG, Hu F, Pace TW, Raison CL, Miller AH. Endogenous glucocorticoids protect against TNF-alpha-induced increases in anxiety-like behavior in virally infected mice. Molecular psychiatry. 2007; 12:408–17. [PubMed: 17389906]

Simard JM, Chen M, Tarasov KV, Bhatta S, Ivanova S, et al. Newly expressed SUR1-regulated NC(Ca-ATP) channel mediates cerebral edema after ischemic stroke. Nature medicine. 2006; 12:433–40.

Sonnen JA, Larson EB, Crane PK, Haneuse S, Li G, et al. Pathological correlates of dementia in a longitudinal, population-based sample of aging. Annals of neurology. 2007; 62:406–13. [PubMed: 17879383]

Vinters HV, Ellis WG, Zarow C, Zaias BW, Jagust WJ, et al. Neuropathologic substrates of ischemic vascular dementia. Journal of neuropathology and experimental neurology. 2000; 59:931–45. [PubMed: 11089571]

Wu LJ, Wu G, Akhavan Sharif MR, Baker A, Jia Y, et al. The voltage-gated proton channel Hv1 enhances brain damage from ischemic stroke. Nat Neurosci. 2012; 15:565–73. [PubMed: 22388960]

Xuereb JH, Brayne C, Dufouil C, Gertz H, Wischik C, et al. Neuropathological findings in the very old. Results from the first 101 brains of a population-based longitudinal study of dementing disorders. Annals of the New York Academy of Sciences. 2000; 903:490–6. [PubMed: 10818543]

Zador Z, Stiver S, Wang V, Manley GT. Role of aquaporin-4 in cerebral edema and stroke. Handbook of experimental pharmacology. 2009:159–70. [PubMed: 19096776]

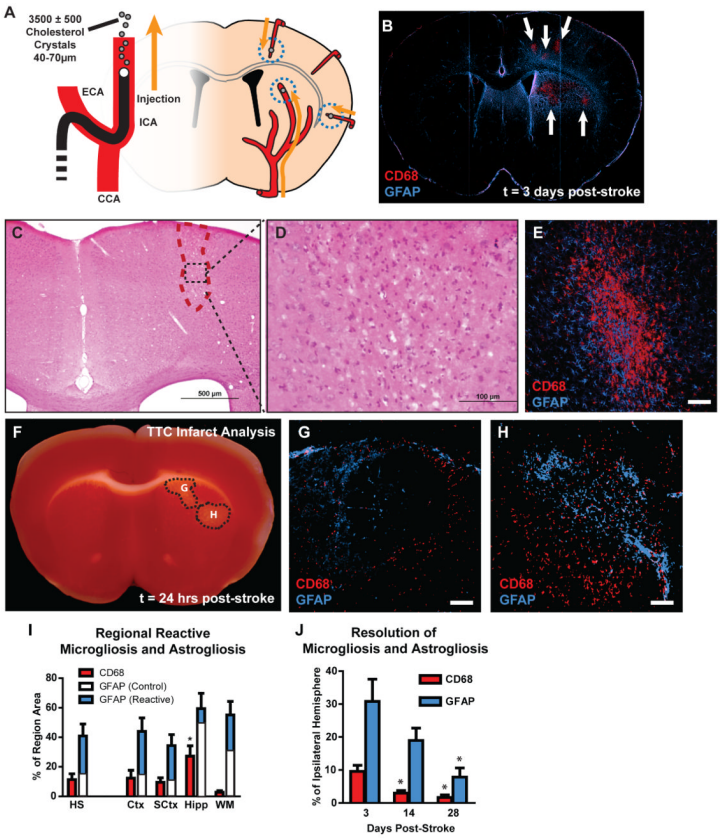

Figure 1. Widespread reactive gliosis surrounding diffuse ischemic lesions

(A) Schematic of diffuse stroke model. 3500±500 cholesterol crystals (40-70μm) are injected unilaterally via the internal carotid artery (ICA). Ischemic lesions form along the deep segments of penetrating cerebral arteries. **(B)** Ischemic lesions (arrows) are defined by immunolabeling against CD68 and GFAP. Lesions consist of CD68-poisitive cores surrounded by large areas of reactive astrogliosis. **(C-D)** H&E staining 3 days post-injury indicates a small columnar cortical lesion that with marked macrophage infiltration. **(E)** CD68/GFAP immunolabeling of a consecutive slice demonstrates that microinfarcts apparent by H&E labeling are characterized by a CD68-positive core surrounded by a wide field of reactive astrogliosis. **(F-H)** TTC staining and immunolabeling against CD68 and GFAP 24hrs post-stroke shows that lesions are detectible by TTC, and at this time point are surrounded by a rim of reactive microglia and astrocytes. **(I)** 3 days after stroke, CD68-immunolabeling (red bars) occupied a larger proportion of the hippocampus (Hipp) than other brain regions (*P<0.05, ANOVA). GFAP-immunoreactivity (blue bars) occupied large areas surrounding CD68-positive cores. White bars reflect control GFAP-immunoreactivity in contralateral hemisphere. **(J)** 14 days after ischemic injury, CD68-positive lesions occupied a smaller proportion of the ipsilateral hemisphere compared to 3 days (*P<0.05, ANOVA). GFAP-immunoreactivity was not significantly reduced from levels at 3 days until 28 days post-stroke (*P<0.05, ANOVA). Common carotid artery (CCA), external carotid artery (ECA), hemisphere (HS), cortex (Ctx), subcortical regions (SCtx), subcortical white matter (WM). Scale bar: 50μm.

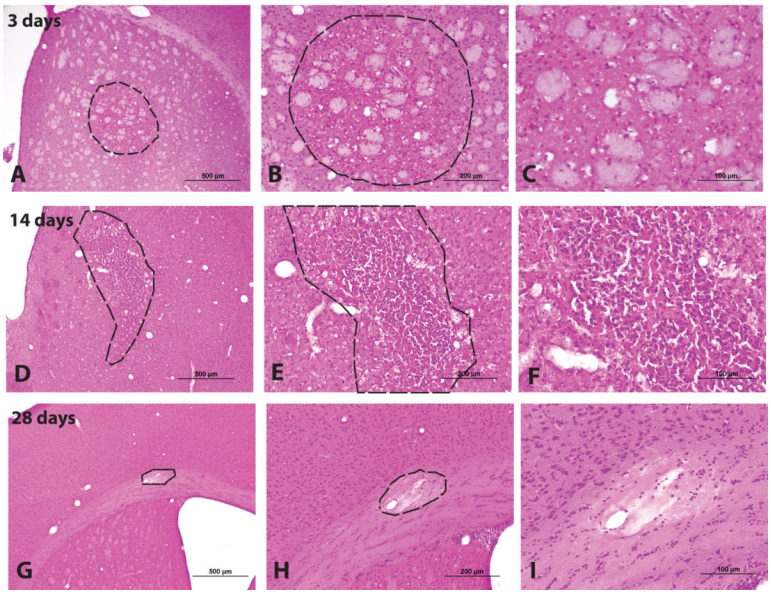

Figure 2. Characterization of diffuse microinfarction by H&E staining

Microinfarcts were evaluated by H& E staining 3 days, 14 days and 28 days post-injury. **(A-C)** At 3 days post-injury, macrophage infiltration into the lesion site is evident. **(D-F)** 14 days post-injury, fibrillary gliosis and pyknotic neuronal nuclei are observed. **(G-I)** Within 28 days post-injury, some cavitated lesions are surrounded by a defined glial scar and have become cystic.

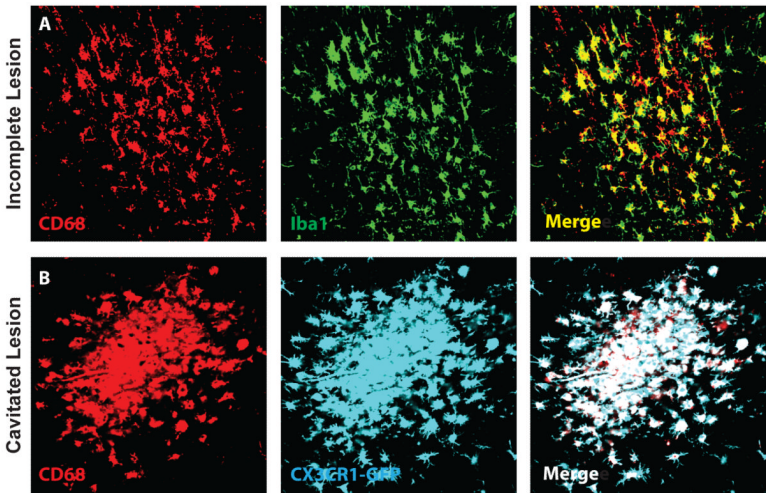

Figure 3. Confirmation of peri-lesional CD68 labeling with other microglial/ macrophage markers

Diffuse CD68 labeling of reactive microglia and infiltrating macrophages in incomplete and cavitated microinfarcts was confirmed **(A)** by double-labeling with the microglial/ macrophage marker Iba1. Double labeling revealed extensive overlap between peri-lesional CD68 and Iba1 immunoreactivity. **(B)** CD68 labeling was also conducted in CX3CR1-GFP reporter mice 3 days after diffuse microinfarction. All CD68 labeling co-localized with endogenous GFP fluorescence.

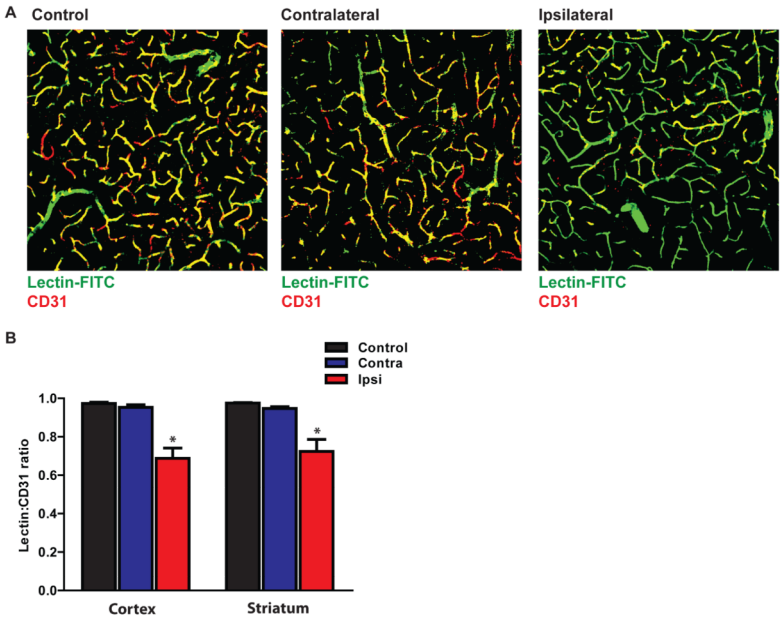

Figure 4. Evaluating the extent of microvascular occlusion after cholesterol crystal injection

Microvascular occlusion was evaluated 1 hr after cholesterol injection by intra-arterial lectin injection and CD31 counter-labeling. **(A)** Representative confocal micrographs depicting CD31-positive vascular endothelium (red), lectin (red)-positive perfused vessels (yellow). Green vessels represent non-perfused vessels. Images were acquired from the ipsilateral and contralateral hemispheres of sham (control)- and diffuse microinfarction-treated animals. **(B)** Quantification of the extent of lectin-labeling of CD31-microvessels in the cortex and striatum. No significant reduction on vessel perfusion was observed in the contralateral hemisphere. A significant reduction in microvascular perfusion was observed in both the ipsilateral cortex and striatum (*P<0.05 vs. Control; ANOVA).

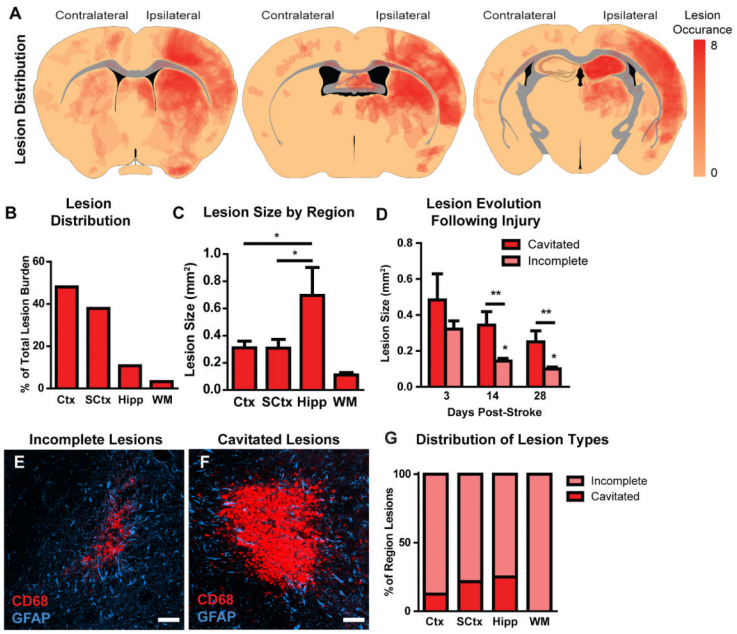

Figure 5. Characterization of diffuse ischemic lesions

(A) Heat map depicting CD68-positive lesion locations, obtained from 8 animals and projected onto 3 representative anatomical slices. <90% of lesions occurred ipsilateral to the cholesterol injection. Note that this represents the aggregate lesion burden across all slices from all animals, and does not represent lesion distribution within a single slice or single animal. **(B)** The greatest proportion of individual lesions was present in the cortex (Ctx) and in the subcortical structures (SCtx). Comparatively few lesions were observed in the hippocampus (Hipp) and the subcortical white matter (WM). **(C)** Lesions within the cortex, subcortical structures and white matter did not differ in size, whereas hippocampal lesions were significantly larger (*P<0.05, ANOVA). **(D)** Diffuse incomplete lesions were significantly smaller in size than dense cavitated lesions (**P<0.01 ANOVA). At 14 and 28 days post-stroke, incomplete lesions were significantly smaller than at 3 days (*P<0.05, ANOVA), while cavitated lesions did not differ significantly at any time point. **(E-F)** Representative confocal micrographs depicting incomplete lesions **(E)** and cavitated lesions (**F**) labeled for reactive microglia (CD68) and reactive astrocyte (GFAP) markers. **(G)** Distribution of incomplete and cavitated lesions throughout different brain regions. Cavitated lesions were most common in the hippocampus and were not observed in the subcortical white matter. Scale bars: 25μm.

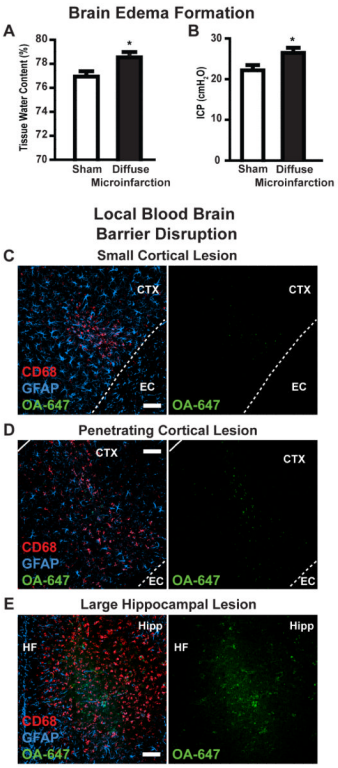

Figure 6. Edema formation and localized blood brain barrier disruption

(A-B) 3 days after diffuse stroke induction, mild cerebral edema formation was observed. Tissue water content in diffuse stroke brains was significantly higher than in sham-treated brains (left; *P<0.05, t-test). Intracranial pressure (ICP) was significantly higher in stroke-treated brains than sham controls (right; *P<0.05, t-test). **(C-E)** Blood brain barrier disruption after stoke was evaluated by imaging extravasation of ALEXA647-conjugated ovalbumin (OA-647, iv administration) in and around CD68- and GFAP-positive lesions. **(C-D)** In small lesions, highly localized blood brain barrier disruption was observed. **(E)** In large lesions, more widespread blood brain barrier was observed. Cortex (Ctx), external capsule (EC), hippocampus (Hipp), hippocampal fissure (HF). Scale bars: 50μm.

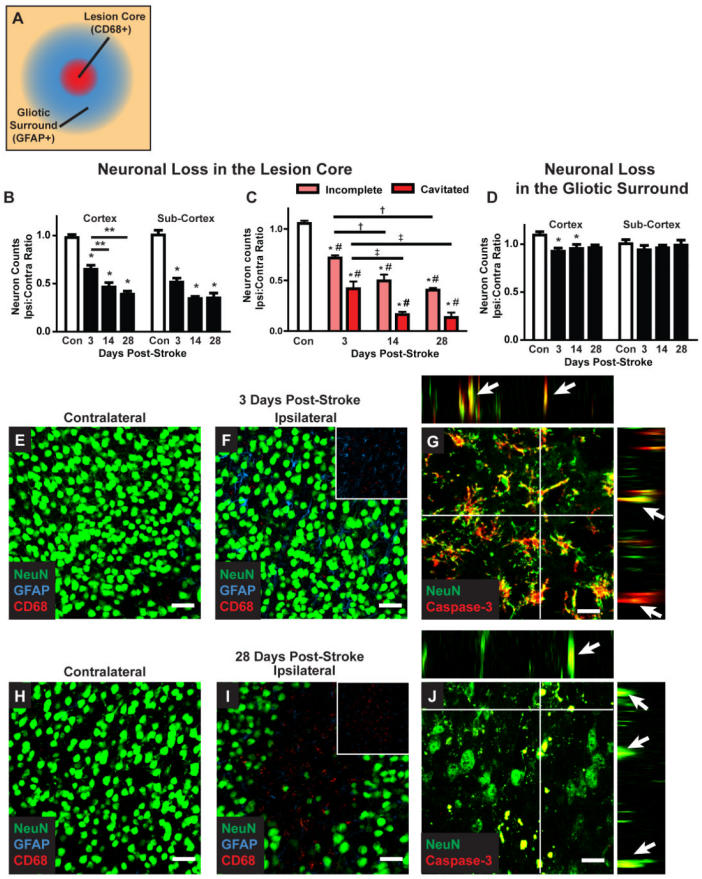

Figure 7. Delayed neuronal cell death after diffuse ischemic stroke

(A) Neuronal cell death was evaluated by NeuN immunolabeling. 40X confocal images (211 × 211μm) were generated centered upon CD68-positive cores of diffuse ischemic lesions and in areas 200um away that are characterized by an extended field of GFAP-positive reactive astrogliosis. All neurons within the image frame were counted. **(B)** Within the CD68-positive lesion, neuronal cell death in the cortex and subcortical regions was significantly reduced 3 days after stroke (*P<0.05, ANOVA). In the cortex, neuronal loss was significantly greater at 14 and 28 days after diffuse injury than at 3 days (*P<0.05, ANOVA). **(C)** When neuronal loss was evaluated based upon lesion type (incomplete vs. cavitated), more rapid and complete neuronal loss was observed in cavitated lesions (*P<0.05, Lesion vs. Control; #P<0.05 incomplete vs. cavitated; †P<0.05 vs. 3 day incomplete; ‡P<0.05 vs. 3 day cavitated; ANOVA). **(D)** In surrounding areas of reactive astrogliosis, a small but significant reduction cortical neuronal counts was observed (*P<0.05, ANOVA). No difference in subcortical neuronal counts was observed. **(E-F; H-I)** Representative confocal micrographs from CD68- and GFAP-positive lesions and mirror-image contralateral control regions 3 days and 28 days post-stoke. Scale bars: 25μm. **(G, J)** Representative NeuN/caspase-3 labeling at 3 and 28 days post-injury shows ongoing neuronal cell death up to 28 days post-injury. Orthogonal views from z-stacks (xz and yz) demonstrate co-localization between NeuN- and caspase-3-immunoreactivity. Scale bars: 12.5μm.

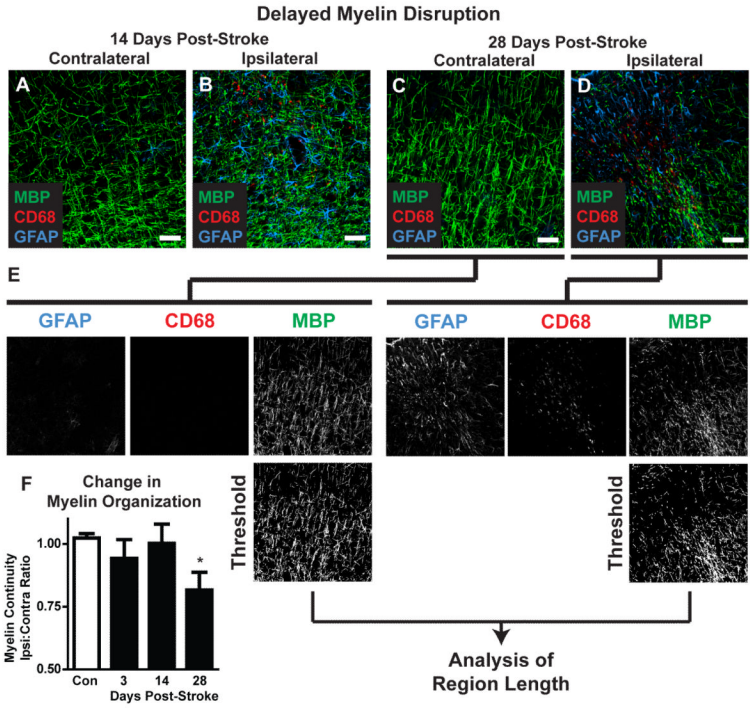

Figure 8. Delayed demyelination following diffuse ischemic stroke

(A-D) Representative confocal images depicting myelin basic protein (MBP) labeling in CD68- and GFAP-positive lesions 3 and 28 days after diffuse stroke injury. **(E)** Changes in myelination were assessed by image analysis. Color channels were split and the MBP channel was background subtracted, uniformly thresholded and converted into a binary image. MBP-positive regions of interest (ROIs) were generated and the length calculated. The median ROI length was calculated and designated as an arbitrary value for 'myelin continuity'. Myelin continuity was compared across time points by expressing the ratio between values measured in ipsilateral lesions:mirror-image contralateral control tissue. **(F)** 28 days after stroke, myelin continuity was significantly reduced compared to control values ($P<0.05$, ANOVA), reflecting delayed myelin degeneration. Scale bars: 25μm.

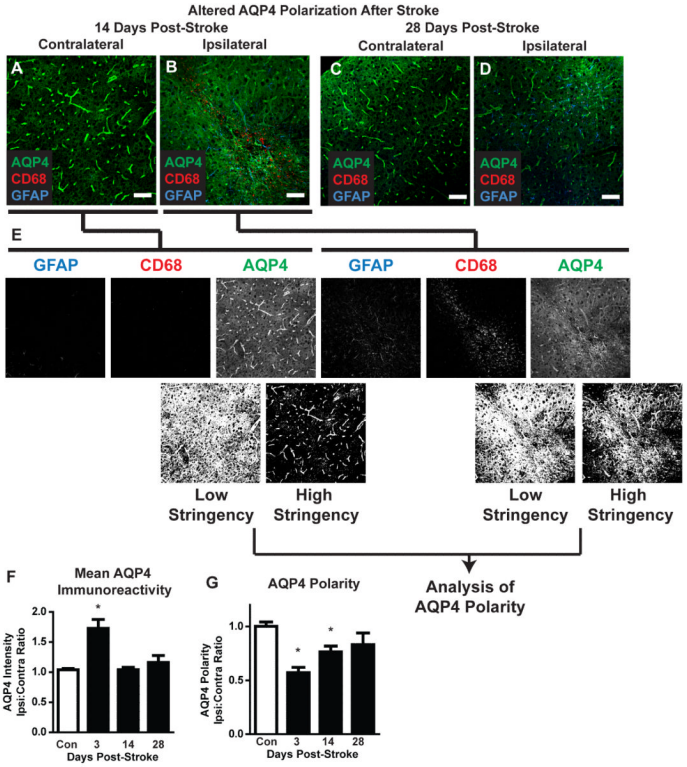

Figure 9. Dysregulation of astrocytic AQP4 expression after diffuse ischemia

(A-D) Representative confocal micrographs showing AQP4 expression and polarization in CD68- and GFAP-positive lesions and in mirror-image contralateral regions 14 and 28 days after diffuse ischemic stroke. **(E)** Changes in AQP4 polarization were measured by image analysis. Color channels were split and the AQP4 channel was uniformly thresholded at two levels: low stringency and high stringency. Low stringency included all AQP4-immunoreactive pixels within the image. High stringency captured all pixels representing perivascular endfeet, in addition to those with equal or greater intensity. An arbitrary value for 'AQP4 polarity' was derived as the ratio between low stringency:high stringency areas. Higher AQP4 polarity values reflected expression levels of AQP4 in perivascular endfeet being greater than in surrounding tissue while lower AQP4 polarity values reflected greater parity between perivascular endfoot AQP4 expression and AQP4 in non-perivascular portions of astrocytes. AQP4 polarity was compared across time points by expressing the ratio between values measured in ipsilateral lesions:mirror-image contralateral control tissue. **(F)** Within 3 days of diffuse ischemic injury, mean AQP4 immunoreactivity was significantly increased compared to control levels (*P<0.05, ANOVA). Mean intensity levels returned to baseline within 14 days of diffuse stroke injury. **(G)** At both 3 and 14 days after diffuse ischemic injury, AQP4 polarization was significantly reduced (*P<0.05, ANOVA) compared to control values. Within 28 days, polarization had returned to control levels. **(C-F)** Scale bars: 50μm.

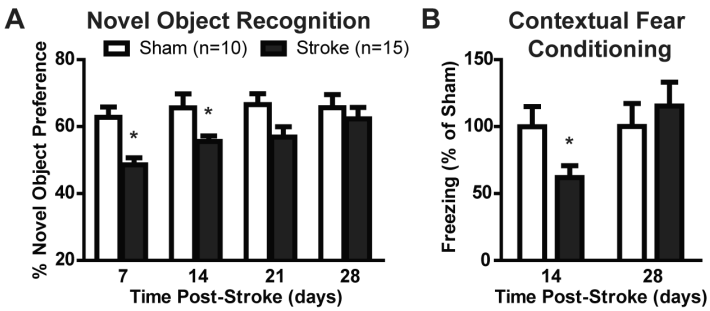

Figure 10. Diffuse ischemic injury results in cognitive decline

(A) 7 and 14 days after diffuse ischemic injury, stroke mice exhibited cognitive decline compared to sham controls in the novel object recognition test ($P<0.05$, ANOVA). By 28 days post-stroke, cognitive function had recovered to control values. **(B)** Cognitive function was also evaluated by the fear conditioning test 14 and 28 days after injury. At 14 days, stroke mice exhibited significant cognitive deficits compared to sham controls (*$P<0.05$, ANOVA), while at 28 days this deficit had recovered.